Design A DIY 3D Scanner for Scanning a 3D Object Using Arduino

Huiying Li[1], Chin Guan Lim[1], Yit Yan Koh[1], Chiang Liang Kok[1]

[1] *University of Newcastle, Australia*
Corresponding Author: chiangliang.kok@newcastle.edu.au

---**ABSTRACT**---
This project is about designing, manufacturing, and experimental verification of an Arduino-based DIY 3D scanner to meet the extensive needs of 3D scanning in manufacturing and reverse modeling. The principles of commercial 3D scanners are mainly based on time of flight, triangulation, and structured light, which are expensive. This project builds a low-cost 3D scanner based on triangulation with a total cost of $ 161.95. Arduino is the central control unit, combined with a lifting platform, rotating platform, infrared distance sensor, SD card storage module, and TFT touch screen. 3D scanner adopts a modular approach to establishing circuits, effectively reducing the consumption of circuit consumables. For the electrical part, the project proposes a low-pass hardware filtering method for the infrared sensor and a software filtering method for processing value obtained from the sensor, which significantly improves the scanning accuracy. For the mechanical part, establishing a digital model of a portable system in SolidWorks has made it possible to reduce the size of industrial-grade 3D scanners. The scanned data of the scanned object will be stored in the SD card for data transmission. The software part uses the SolidWorks (ScanTo3D) software to process the obtained point cloud data and generate high-quality 3D models. After the scanning test of this project, the root mean square error (RMSE) and mean absolute error (MAE) of the regular sample size obtained by the scanner are 1.6539 and 1.4056, respectively. Therefore, the scanner's precise scanning accuracy facilitates the digital management of simple objects.

KEYWORDS;- *3D scanner, Reverse engineering, Arduino*

Date of Submission: 10-12-2023   Date of acceptance: 25-12-2023

I. INTRODUCTION

With the development of computer technology and optical technology, three-dimensional scanning technology is incredibly beneficial for reverse engineering, heritage protection, medicine, and other fields. The working principle of the 3D scanner is mainly to achieve the reverse modeling of objects by emitting laser or structured light and then acquiring the geometric features of the object surface through the camera, including coordinates, color information, and reflection intensity [1]. The non-contact high-speed laser measurement method allows for rapid scanning and measurement of complex objects without damaging them. Although 3D scanning technology is widely used in various fields, there are still shortcomings in data accuracy or scanning speed [2]. Due to the continuous improvement of modern manufacturing processes and product design levels, the precision of products has made manual measurement increasingly difficult. Especially for some components with multiple structures and features, it is almost impossible to obtain complete product data through manual measurement [3]. Reverse engineering is obtaining point cloud data by 3D scanner on the object's prototype, then transferring the data to the computer to construct a 3D model with the same shape and structure after software processing. Then, modify the original form or redesign and innovate based on the original form.

II. LITERATURE REVIEW

The 3D scanner is mainly divided into contact and non-contact, and the most typical contact 3D scanner is a Coordinate Measuring Machine (CMM) [4]. The measuring machine has two movable guide rails and scales on the x-axis and y-axis, as well as displacement sensors on the z-axis. The coordinate-measuring machine uses a probe to measure the coordinates of a point on an object. For large and complex surfaces, its scanning process can be very cumbersome. In addition, using contact measurement may damage the probe and the surface of the measured object's surface. Non-Contact 3D scanners mainly include triangulation scanners, phase-shifting scanners, computer tomography, etc. After the successful development of the laser by Mayman, a scientist at Hughes Aircraft Company, in 1960, the laser was used to measure distance [5]. Laser laid the foundation for the development of laser 3D scanners. Measuring the reflection time and position of the laser

beam was used to obtain the point cloud data of objects. Since measuring the distance of a single point every time, it took a lot of time to scan things.

In 1992 Strauss proposed a 3D perception system based on the structured light sensor. The projector projects multi-stripe patterns, grids, or multiple points to greatly reduce the time of scanning objects [6]. When the structured light scanner scans, the grating projection device projects several specially coded structured lights onto the object to be measured, and two cameras with a certain included angle synchronously acquire the corresponding images. Then, computer software decodes and calculates the phase of the image and uses matching technology and triangle measurement principles to calculate the three-dimensional coordinates of pixels in the standard viewing area of the two cameras [7]. Even though the scanning time can be reduced, structured light is vulnerable to being affected under certain conditions, such as sun exposure. Therefore, the use of structured light 3D scanners is still limited. The brands of structured light scanners on the market with accuracy up to 0.1mm include Revopoint, Creativity, Shining 3D, etc. Their prices are approximately 600 to 1000 US dollars. The scanner based on laser triangulation with the same accuracy costs 800 to 1200 US dollars [8]. For personal use, the price is relatively high. For such a high price, this project will provide a solution for a small 3D scanner that individuals can easily set up. Using low-cost, reliable hardware and Open-source software can significantly reduce the overall product cost compared with commercial scanners on the market.

Using the triangulation method to realize precise 3D scanning is feasible for scanning small objects. In addition, for cost control, triangulation distance sensor GP2Y0A02YK0F is adopted for scanning, and the Nema17 stepper motors with a rotating table control XY direction and a ball screw nut control Z direction to achieve positioning function. By controlling different motion axes, Arduino enables the sensor to realize multi-dimensional scanning and measurement to capture more comprehensive surface features of the object. After scanning, all the scanned data will be stored in the SD card for data transfer for SolidWorks post-processing.

III. METHOD AND METHODOLOGY

The Arduino-based low-cost scanner is designed as a suitcase (see Figure 1), so it is tiny and portable.
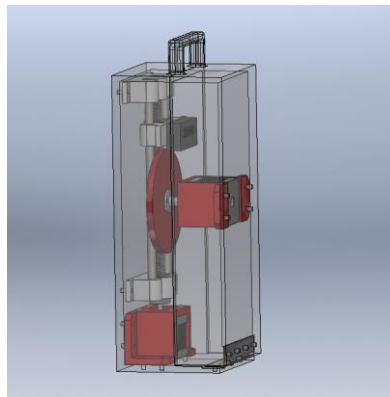

Figure 1 The shape of the scanner

The main mechanical structure of the scanner consists of two parts: the screw nut sliding table structure related to the Z-axis and the XY-axis rotating table structure. In addition, the infrared sensor must be fixed on the slide (see Figure 2). As for the mechanical parts of the scanner, except for the supporting optical axis, screw rods, and nuts, which are purchased, the other parts are all 3D printed.
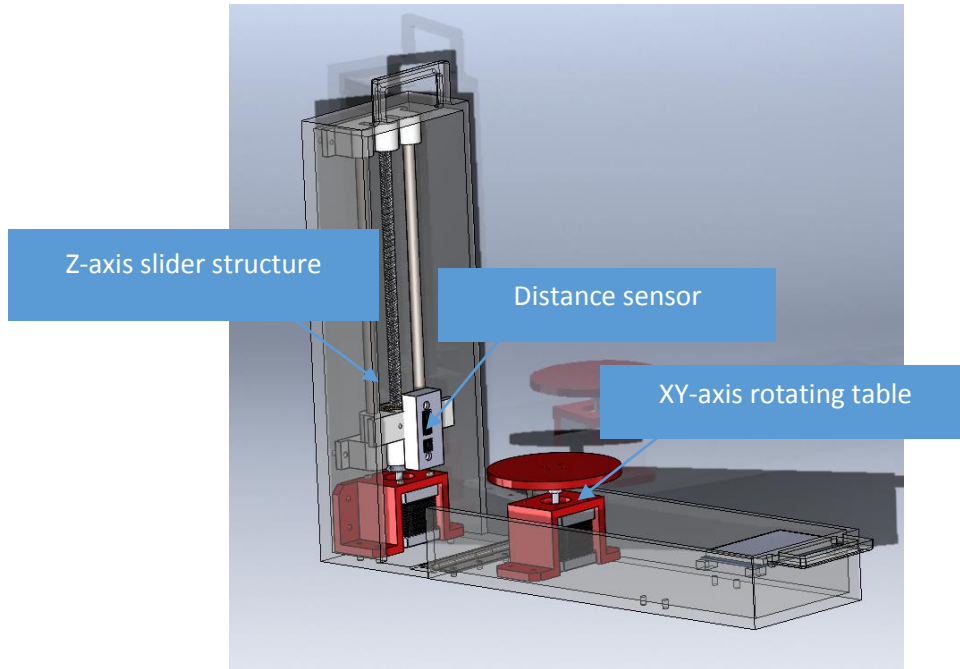
Figure 2 Outline structural diagram

The Arduino mega 2650 is the main control board, and two A4988 stepper motors drive two 42BYGH48 stepper motors. In addition, the core part is a Sharp infrared distance sensor, an SD card module, and a display screen. This project uses an external 12-volt DC power supply for two stepper motors. The 12-volt voltage is then converted to 5 volts using a DC buck converter to power two A4988 stepper motor drives, an SD card module, and an infrared distance sensor. Figure 3 and Figure 4 show the wiring diagram and schematic diagram.
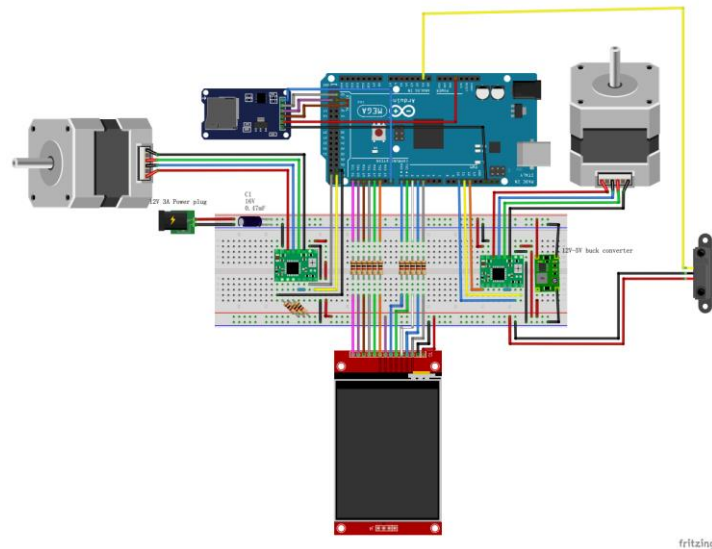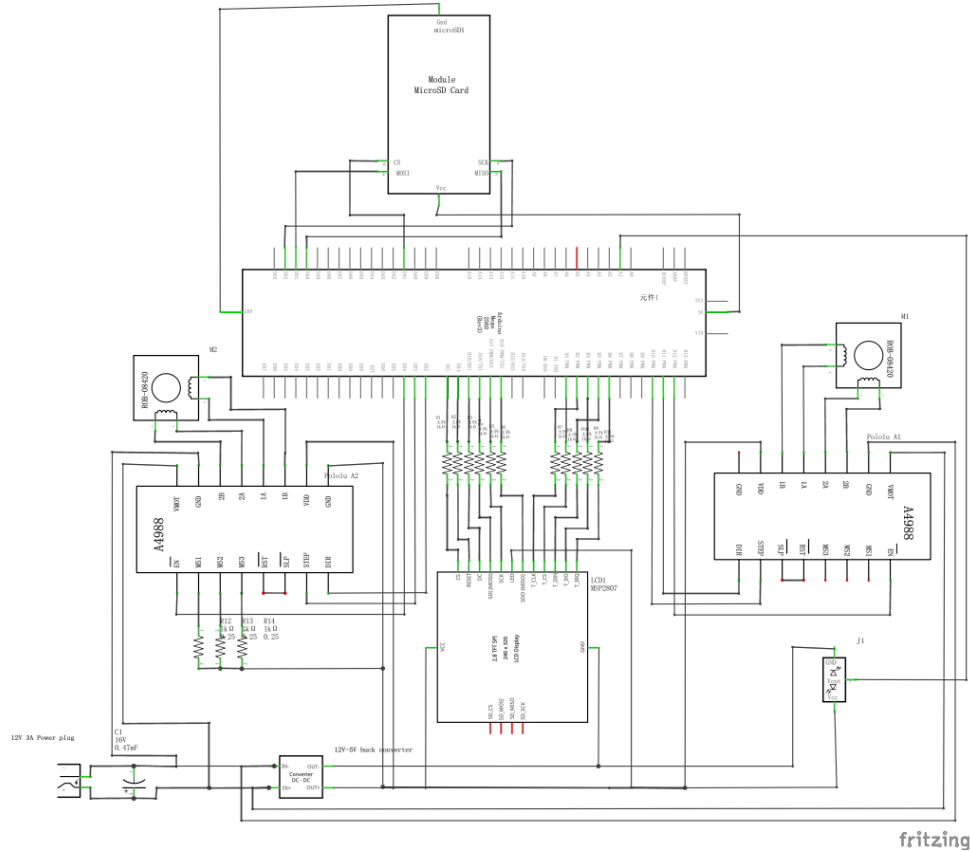

Figure 3 Wire diagram

Figure 4 Schematic diagram

The electronic part of the 3D scanner in this project mainly consists of Arduino mega 2560, Sharp distance sensor (GP2Y0A41SKOF), $12\,V$ to $5\,V$ DC buck converter, SD card module, Stepper motor (42BYGH40S) and ILI9431 2.8-inch capacitive touch screen. The touch screen plays a crucial role in this project, controlling the start of the entire program and displaying the status of the scanner to the user, such as displaying whether the SD card module is connected properly. When the user presses the start button, the display screen displays the text 'Scanning…'. When the scanning is completed, the display screen displays a green hook to indicate the end of the scanning. At the same time, the slide drives the sensor back to the initial position, and the interface displays ready to scan to indicate that the scanning program can be run by pressing the start button again. The Figure 5 displays the flow chart of the touch screen.
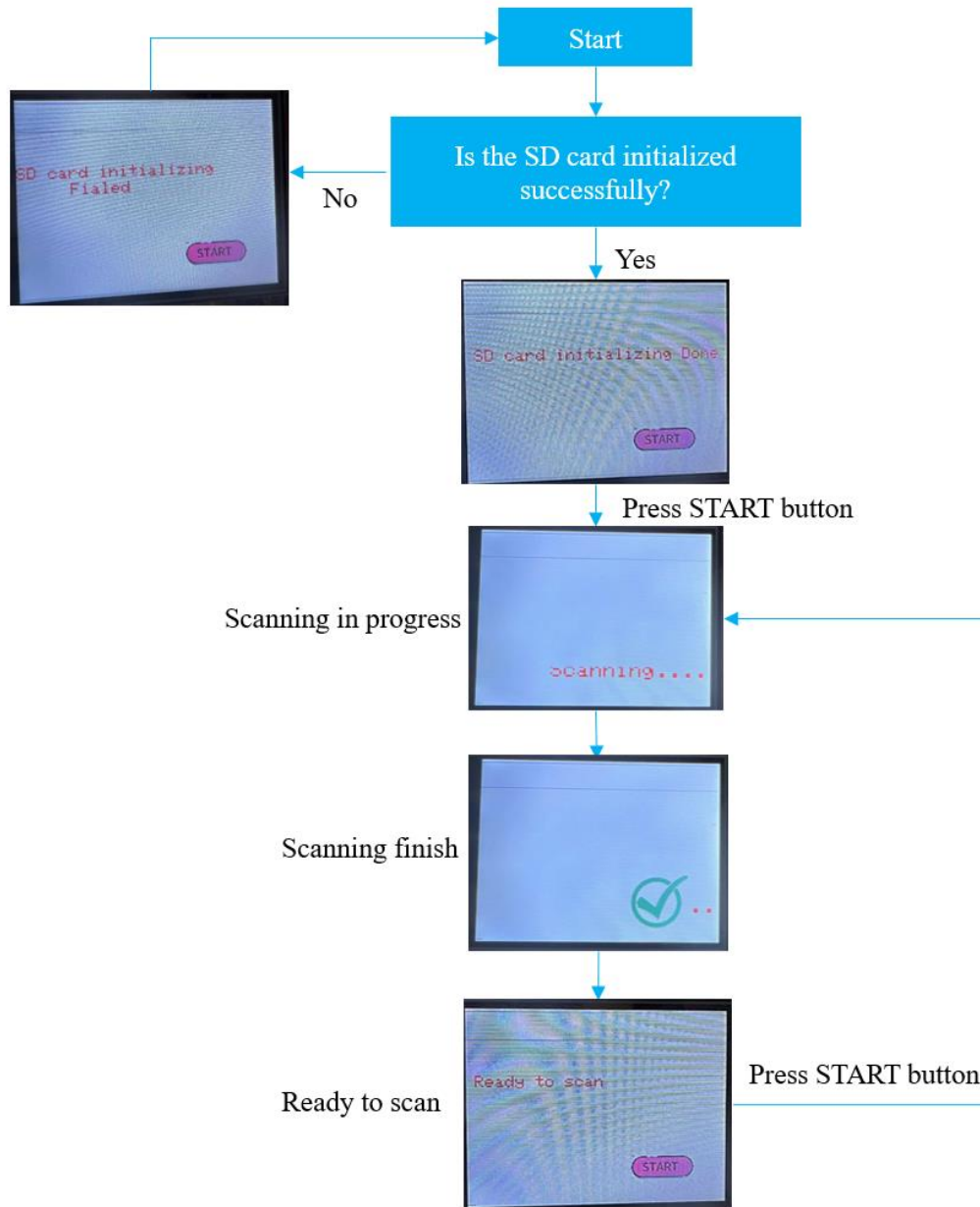
Figure 5 Touch screen display flow chart

When the SD card module, two A4988 drivers, two step motors, and display screen are connected, the input voltage of the Sharp infrared distance sensor GP2Y0A41SKOF has 94 mV ripple interference (see Figure 6) at the measure point in Figure 2.7.
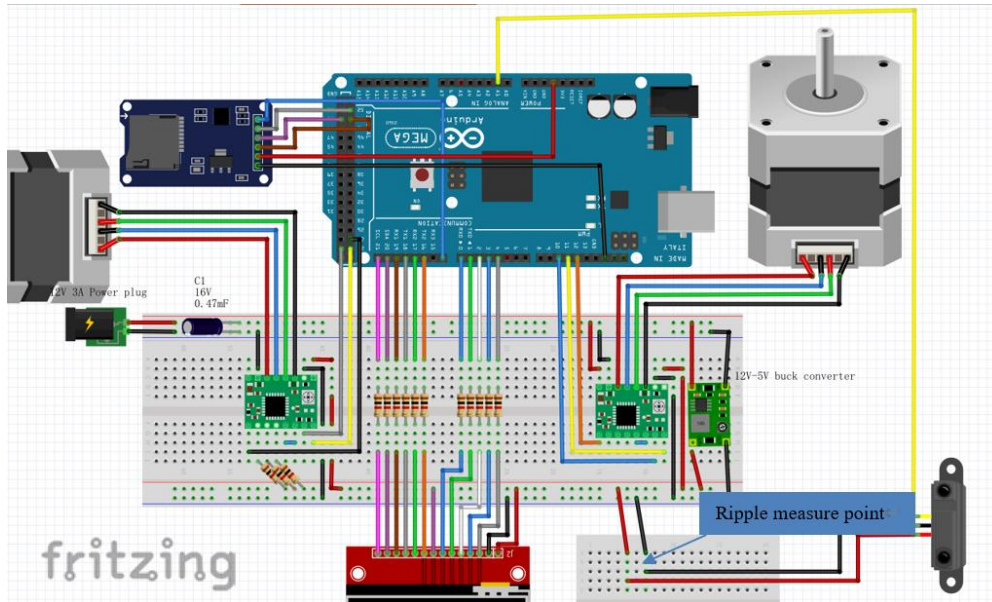
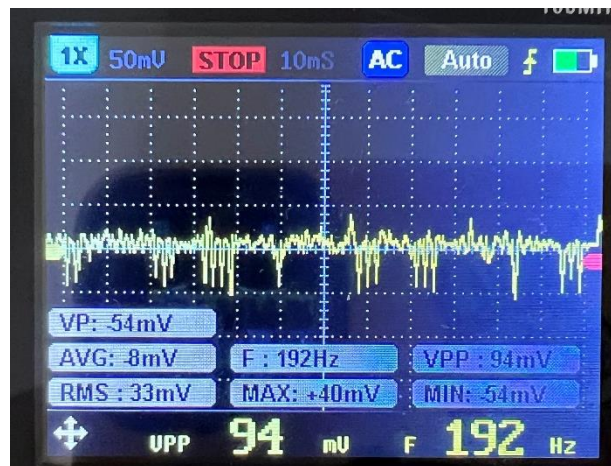Figure 6 Measuring point of ripple of voltage supply

Figure 7 Ripple of voltage supply to Sharp infrared distance sensor

In order to reduce ripple and make the power supply more stable, it is necessary to filter the power output. The working current of the infrared distance sensor (see Figure 2.8) is known to be 11.6 mA, the peak to peak value V_{pp} of the power supply is 94 mV, and the frequency is 192 Hz (see Figure 7). The filtering capacitance value can be calculated by Equation (1).

Figure 8 Working current of the GP2Y0A41SKOF

$$C = \frac{I}{2 \times f \times V_{pp}} = \frac{0.0116}{2 \times 192 \times 0.094} = 321.365 \mu F \tag{1}$$

where C is the capacitance, measured in F, I is the current, measured in A, f is the frequency, measured in Hz, V_{pp} is the peak to peak value of voltage, measured in V.

According to the calculation, the filtering capacitance is $321.365\ \mu F$, so a $330\ \mu F$ capacitor is added to the power supply of the infrared sensor for filtering (see Figure 9). Measure the output ripple of the power supply with added capacitance using an oscilloscope (see Figure 10) to be $52\ mV$, which reduces the ripple of voltage supply for the distance sensor.
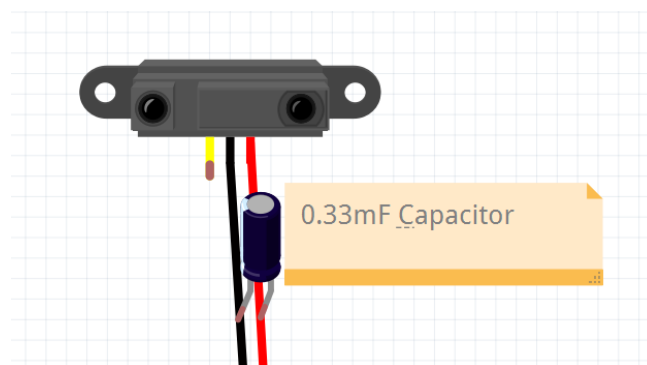

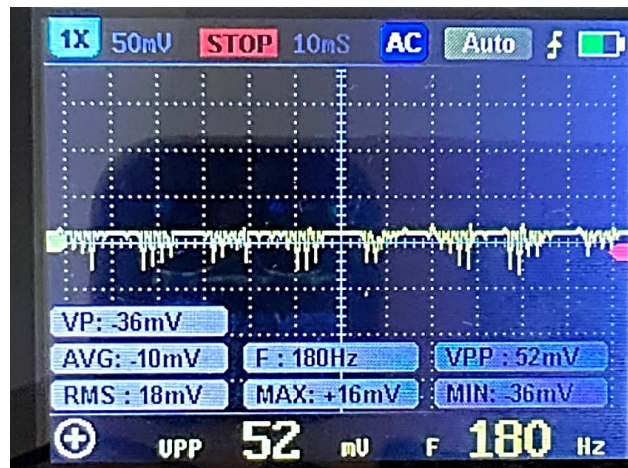Figure 9 Power supply diagram of the distance sensor

Figure 10 Voltage ripple after adding a 330 μF

Figure 11 shows the picture of the experimental setup. Place a white object 13 cm in front of the sensor under regular operation and measure the voltage output by the infrared distance sensor from the measurement point in Figure 12. As shown in Figure 2.13, the output voltage is very noisy, with a peak-to-peak value of 528 mV and a frequency of 60 Hz.
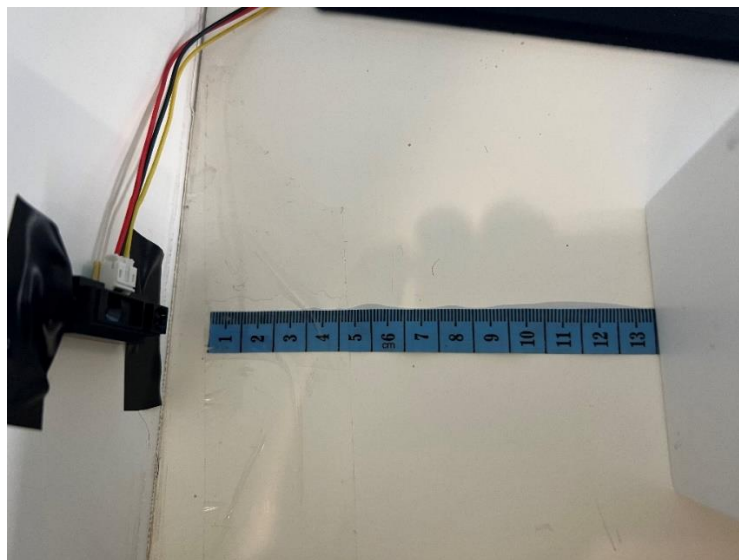

Figure 11 Picture of experimental setup
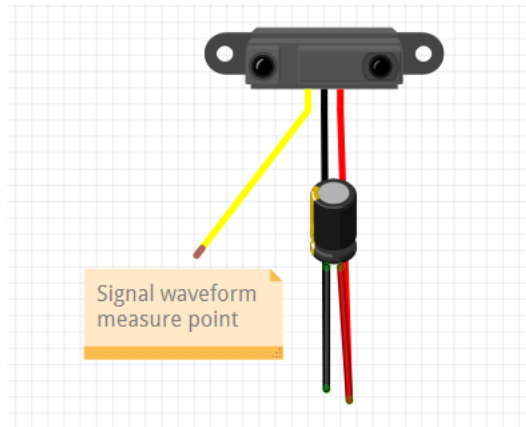
Figure 12 Voltage output of distance sensor

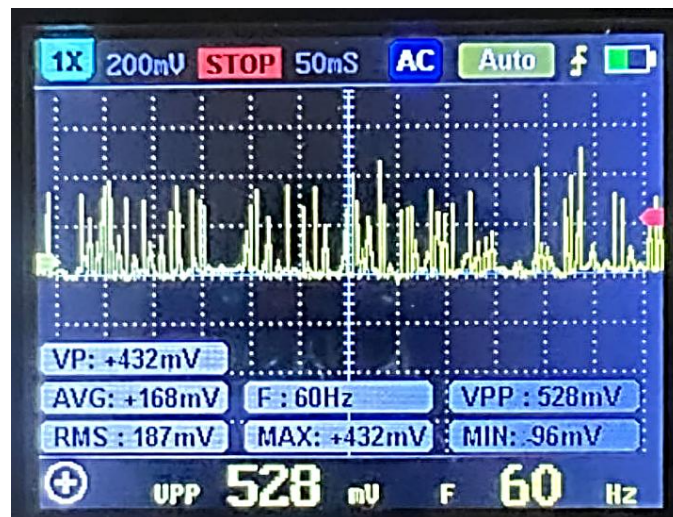Figure 13 Signal waveform of IR sensor

The use of RC low-pass filtering can cut off waveforms above a certain frequency, thus eliminating voltage spikes at a frequency of 60 Hz as shown in the Figure 13 to make the output voltage smoother. For the low-pass filter (see Figure 14), the resistance is 1000 Ω and the capacitance is 4.7 μF. The cut off frequency can be calculated by Equation 2.
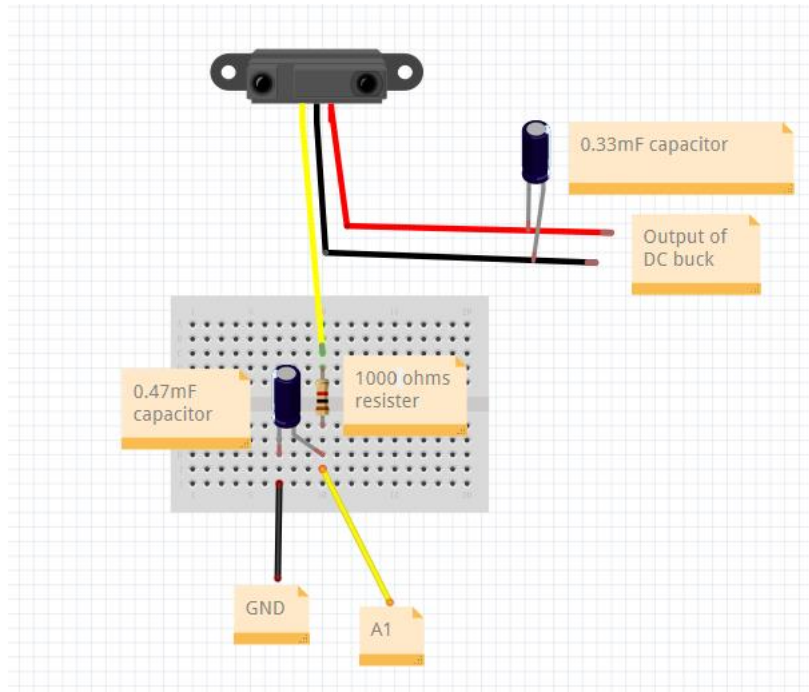
Figure 14 Low-pass filter wiring diagram

$$f_c = \frac{1}{2\pi RC} = \frac{1}{2\pi \times 1000 \times 4.7 \times 10^{-6}} = 33.8628\ Hz \qquad (2)$$

where f_c is the cutoff frequency, measured in Hz, R is the resistance, measured in Ω, C is the capacitance, measured in F.

The frequency of the filter is $33.8628\ Hz$. After low-pass filtering, the signal output of the infrared sensor is smoother, with a peak to peak value (see Figure 15) of only $38\ mV$.
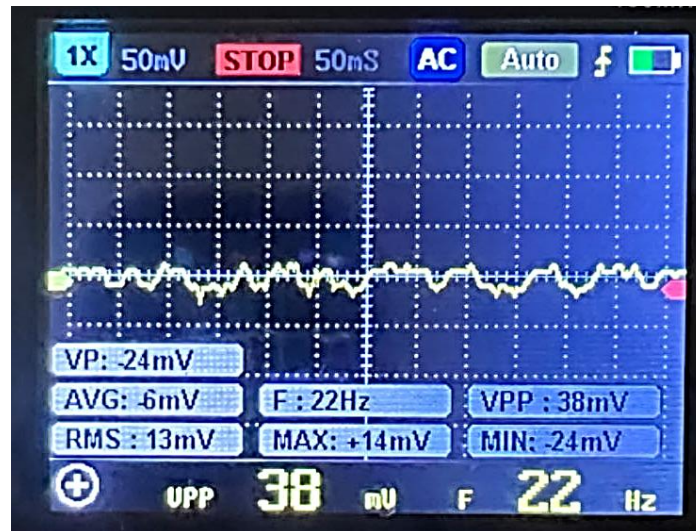
Figure 15 Signal waveform after filtering

Due to the setting of low-pass filtering, the output voltage of the sensor will decrease, resulting in the voltage and distance values provided by Sharp's official data not being applicable. Therefore, it is necessary to measure the distance of the sensor corresponding to the output voltage. Figure 16 shows the experimental set up.
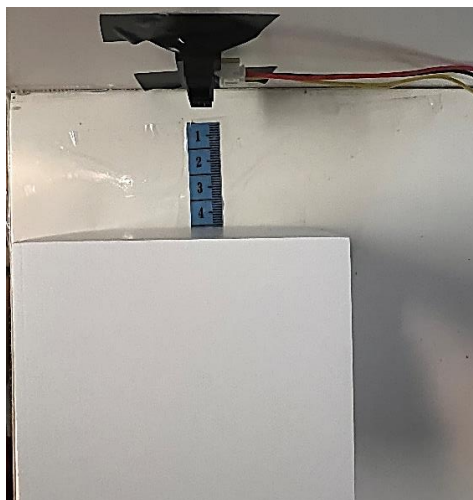
Figure 16 Experimental installation test pictures

Use a multimeter to record the output voltage of Sharp's GP2Y0A41SKOF distance sensor at each measuring distance point in Table 1.

Table 1 GP2Y0A41SKOF sensor output voltage at different distances

Volt（V）	Distance（mm）
2.568	40
2.161	50
1.881	60
1.64	70
1.47	80
1.302	90
1.209	100
1.093	110
0.999	120
0.933	130
0.875	140
0.815	150
0.775	160
0.718	170
0.679	180
0.637	190
0.597	200
0.578	210
0.541	220
0.523	230
0.499	240
0.47	250
0.46	260
0.441	270
0.421	280
0.402	290
0.382	300

Figure 17 Voltage Vs. Distance curve of GP2Y0A41SKOF sensor

As can be shown in Figure 17, the output voltage and distance exhibit a non-linear relationship, and polynomial fitting is used to obtain Equation 3 for the data.

$$y = 36.824x^6 - 348.01x^5 + 1341.3x^4 - 2728.4x^3 + 3171.3x^2 - 2130.6x + 779.28$$

(3)

where y is the distance, measured in mm, x is the voltage, measured in V.

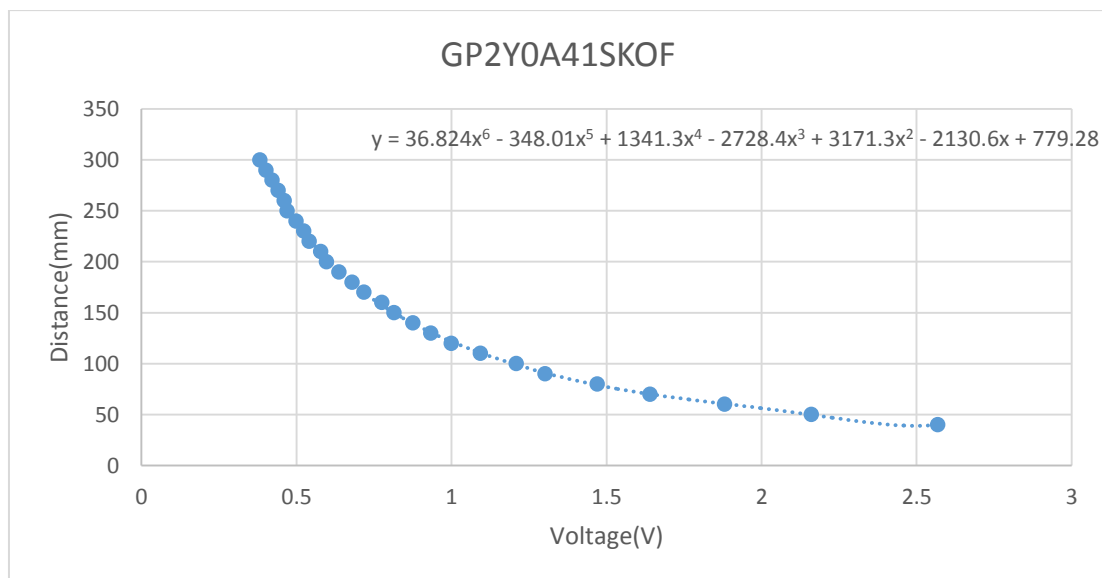There is software filtering way to increase the stability of the measurement, which is to measure 20 times and take the average measurement. Under the same illumination, output 200 measurement results using the same obstacle at a distance of 10 cm from the sensor. The Figure 2.28 shows the comparison between the results of 1 scan and the average of 20 scans. After comparing the images, the combination of low-pass filtering and average filtering method yields the most stable data, with an upper and lower error of about 1 mm.
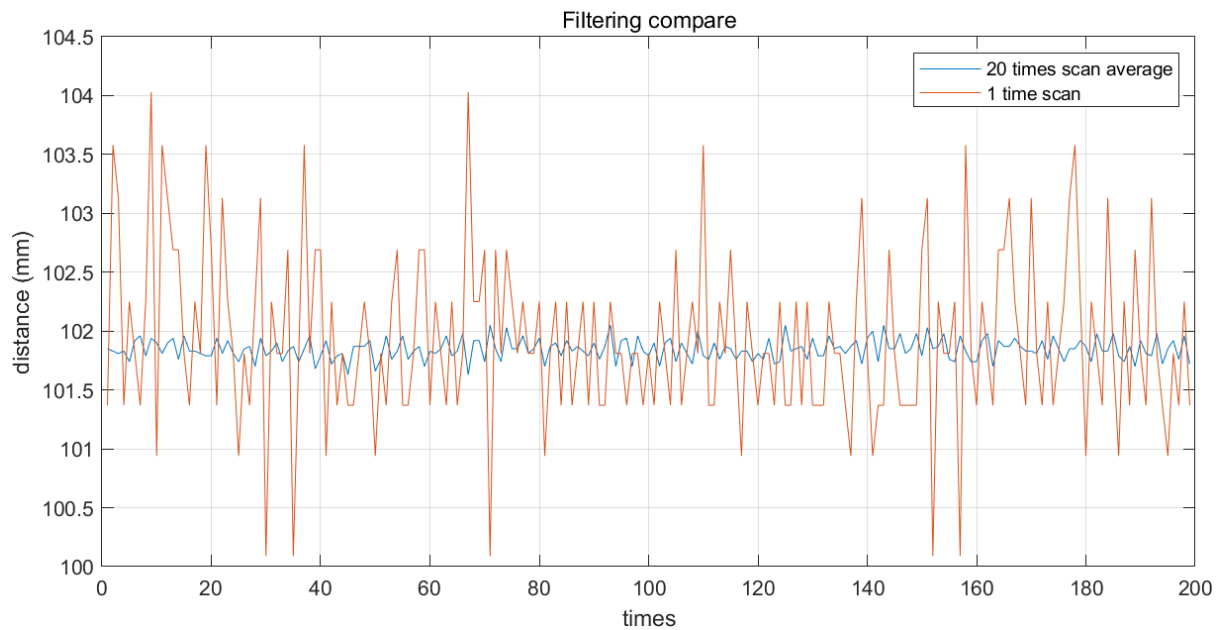
Figure 28 Diagram of filtering compare

Standard deviation in Equation (4) is a measure of how dispersed a set of data is from the mean. The smaller the standard deviation, the less discrete the data. The standard deviation of 20 measurements is calculated by as 0.089, and the standard deviation of 1 measurement is 0.7242. Thus, the result of 20 measurements is more stable than the result of 1 measurement.

$$S = \sqrt{\frac{\sum_{i=1}^{n}(x_i - \bar{x})^2}{n-1}}$$

(4)

$$S_1 = 0.7242$$

$$S_{20} = 0.089$$

Where S is the standard deviation, n is the value of sample, x_i is the value of each sample, $\bar{x}$ is the average value of total sample, S_1 is the standard deviation of 1 measurement, S_{20} is the standard deviation of 20 measurements.

The suitcase shell and parts of the 3D scanner are made of 3D printing. For the mechanical part, the fixing methods are bolt fixing and glue fixing (see Figure 29).
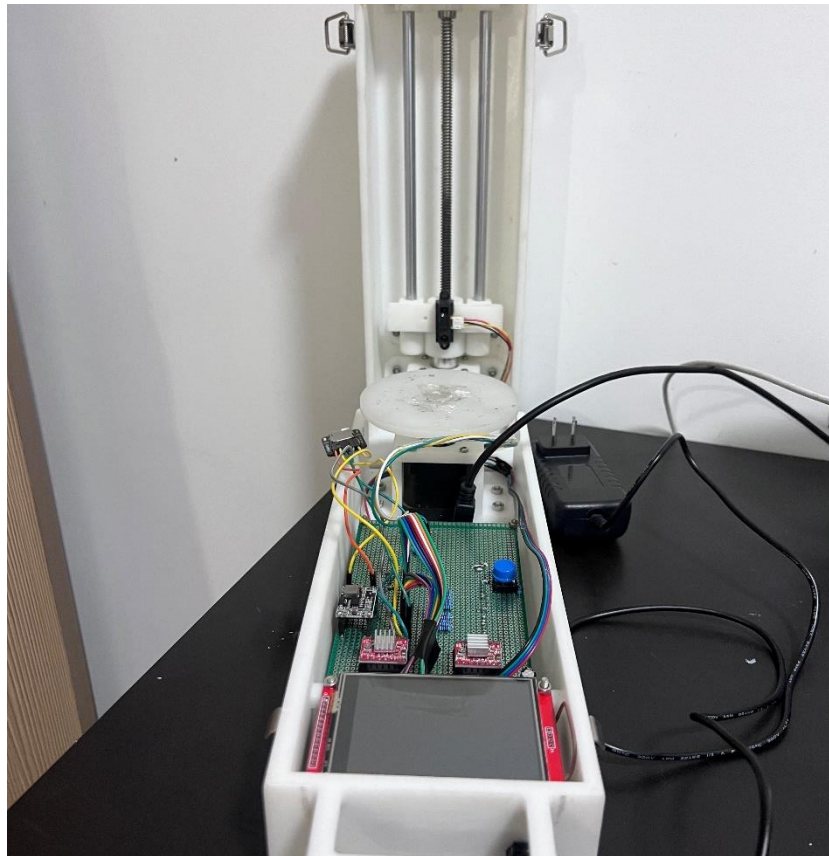
Figure 29 Physical picture of the complete assembly of the 3D scanner

For the circuit part, use jumpers to connect to external modules such as SD card storage modules, display screens, stepper motors and infrared sensors. In addition, in order to reduce the size and prevent poor contact, as can be seen in Figure 30, the Arduino mega 2560 is soldered on the back of the solder board, while the A4988 stepper motor driver, DC-DC step-down module and low-pass filter system are soldered on the front of the solder board. The above electrical components are all connected to each other by wire soldering.
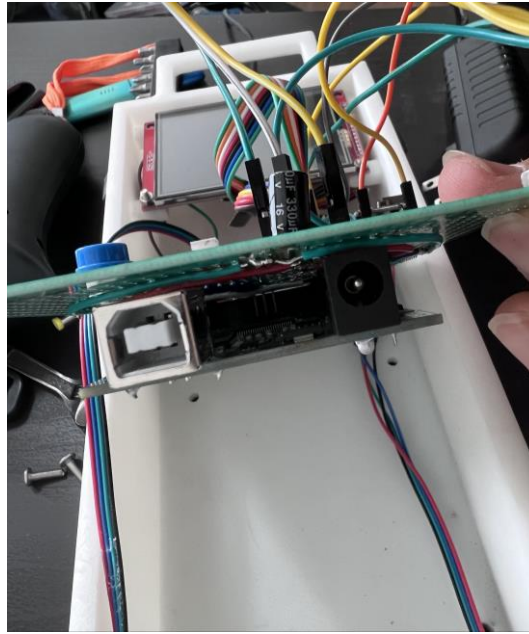
Figure 30 Physical picture of the circuit connecting of the 3D scanner
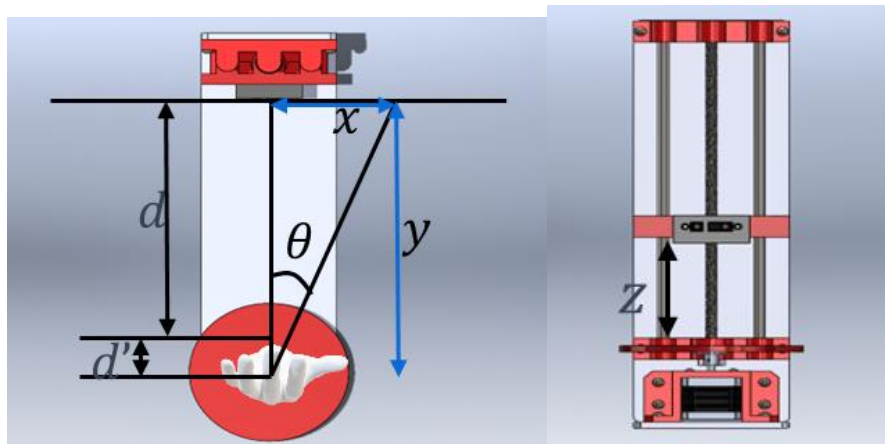
Figure 31 Algorithm diagram

The distance (d) from the center of the object to the sensor is fixed, and the Angle of rotation (θ) of the disk is also fixed. Therefore, the distance from the object contour to the midpoint (d') can be calculated from the measured distance (see Figure 31). The x, y coordinates of the measured point can also be derived from the Equation (5) and (6). Z coordinate is the lifting distance of the distance sensor.

$$x = \sin(\theta) \times d' \tag{5}$$

$$y = \cos(\theta) \times d' \tag{6}$$

where x, y are coordinates, measured in mm, d' is the distance from the scanned object to the midpoint of the rotating table, measured in mm, θ is the angle of rotation, measured in °.

The scanning program is set to start scanning when the start button on the screen is pressed and the sensor detects an object being scanned. The infrared ranging sensor and the XY axis stepper motor operate alternately. When the XY axis stepper motor completes one full turn, the Z-axis motor rotates, causing the infrared sensor to lift, and then repeats until the infrared sensor cannot detect an object, that is, the scanning is completed. Finally, the Z-axis motor runs in reverse to return the sensor to its original position. During this scanning period, once the object is moved, the scanning will stop, and the sensor will return to its original position. All scanner operation flow charts are shown in Figure 32.
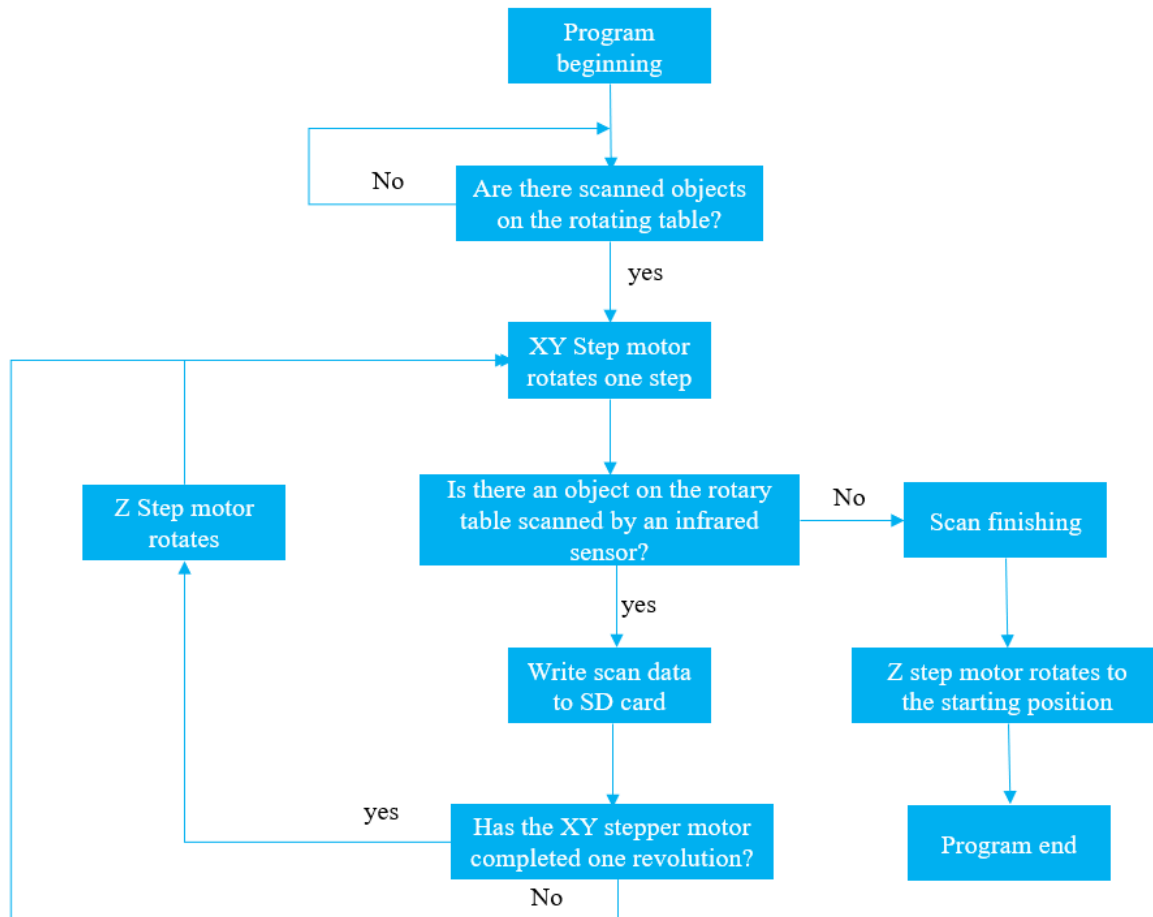
Figure 32 Program flowchart

In order to verify the scanning accuracy and performance of the scanner, regular sample 1,2,3 made of resin and an irregular sample were scanned by three times under the same lighting environment. The scanning mode of the scanner is 200 steps per complete turn (1.8 ° per step) for the XY-axis motor, and the Z-axis sliding table is raised by 2 mm each time.

The performance verification method uses a caliper to measure the size of the sample as a reference standard and compares the results with the data scanned by the scanner and processed by SolidWorks (ScanTo3D) to calculate the error.

Use digital calipers to measure data at the marked points of regular sample 1, 2, 3 and an irregular sample. To reduce the measurement error, the distance between each point is measured three times and recorded, and the average value in is calculated as the reference size of the model. Figures 33 shows the marked points of regular samples 1, 2, 3 and Figure 34 shows an irregular sample.

Figure 33 Marking point of sample 1, 2, 3

Figure 34 Marking point of irregular sample

The data obtained by scanning with the 3D scanner for this project is a text file containing the coordinates of each sample. To get the model and size of each sample, it needs to be post-processed with SolidWorks. Therefore, the results of the three scans of samples 1, 2, and 3 were transferred to the computer from the SD card and imported into SolidWorks. Start the ScanTo3D software, and then use the grid wizard to position the imported point cloud to facilitate confirmation of the location of the marker points. The point cloud is then denoised and smoothed to generate a mesh (see Figure 35 and Figure 36). Then, open the surface wizard and select the generated mesh to automatically generate surfaces for each face of the model to complete the reconstruction of models in Figure 37 and Figure 38.
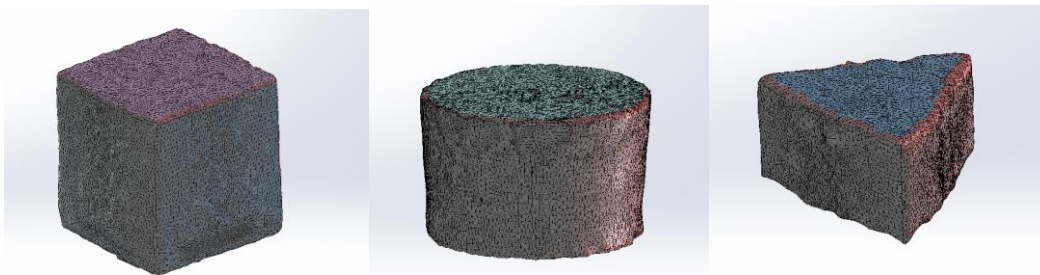

Figure 35 Mesh of sample 1,2,3

Figure 36 Mesh of irregular Sample
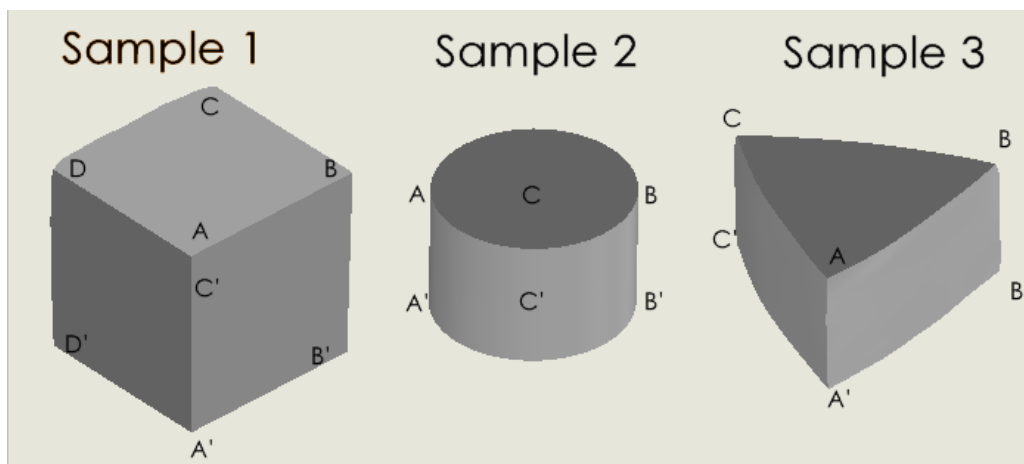
Figure 37 reconstructed surface of sample 1,2,3
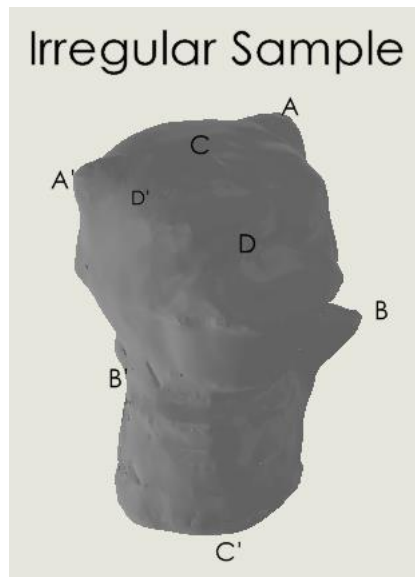
Figure 38 the reconstructed surface of irregular Sample

After reconstructing the model, use SolidWorks to generate engineering drawings for the three reconstructed models of samples 1, 2, 3, and irregular samples and mark the dimensions. For the scanning results of this scanner, root mean square error (RMSE) and mean absolute error (MAE) are used, which are a quantitative trade-off method for judging the error of predicted values (model reconstruction results) and actual values (caliper measurement results).

Each model was scanned three times. Calculate the error between each scan and the caliper measurement in Equation (7) for each point-to-point position.

$$\delta_i = x_{c,i} - x_i \tag{7}$$

Where δ_i is the length error, measured in mm, $x_{c,i}$ is scan results of models for models, measured in mm, x_i is the caliper measurement results of models, measured in mm.

Then, calculate the average error of three scans of the error calculated in Equation (7) in Equation (8).

$$\bar{\delta}_i = \frac{\sum_{i=1}^{n}|\delta_i|}{n} \tag{8}$$

where $\bar{\delta}_i$ is the average error of each scan, measured in mm, n is the scanning times, which is equal to 3.

Based on Equation (8), calculate the RMSE and MAE of each scan of each model in Equation (9) and (10).

$$RMSE = \sqrt{\frac{\sum_{1}^{n}\bar{\delta}_i}{n}} \tag{9}$$

$$MAE = \frac{\sum_{1}^{n}\bar{\delta}_i}{n} \tag{10}$$

where $RMSE$ is the root mean square error, measured in mm, MAE is the mean absolute error, measured in mm, n is the number of measuring points.

Based on the RMSE and MAE calculated by Equations (9) and (10), Equation (11) and (12) calculates the combined RMSE and MAE for samples 1, 2, and 3 to evaluate the scanning accuracy of the scanner for simple objects.

$$RMSE_C = \frac{\sum_{1}^{n}RMSE_i}{n} \tag{11}$$

$$MAE_C = \frac{\sum_1^n MAE_i}{n} \qquad (12)$$

where $RMSE_C$ is the combined root mean square error, MAE_C is the combined mean absolute error.

IV. PESULTS AND DISCUSSION

Tables 2 and 3 show the dimensional measurements at each marking point and the average of three measurements.

Table 2 Caliper measurements of marked points

Sample 1	Caliper1	Caliper2	Caliper3	Mean Caliper(mm)
A–B	79.76	79.53	79.81	79.7
B–C	79.15	79.2	79.13	79.16
C–D	79.62	79.67	79.66	79.65
D–A	79.28	79.26	79.18	79.24
A'–B'	78.97	79.53	77.6	78.7
B'–C'	78.66	78.56	78.82	78.68
C'–D'	79.24	79.25	79.32	79.27
D'–A'	78.69	78.67	78.56	78.64
A–A'	79.49	79.4	79.37	79.42
B–B'	79.63	79.61	79.59	79.61
C–C'	79.49	79.45	79.47	79.47
D–D'	79.37	79.39	79.44	79.4
Sample 2	Caliper1	Caliper2	Caliper3	Mean Caliper(mm)
A–B	75.5	75.43	75.45	75.46
A–A'	50.42	50.39	50.39	50.4
B–B'	50.3	50.28	50.29	50.29
C–C'	50.24	50.21	50.21	50.22
Sample 3	Caliper1	Caliper2	Caliper3	Mean Caliper(mm)
A–B	98.37	98.41	98.39	98.39
B–C	98.52	98.56	98.54	98.54
C–A	98.79	98.77	98.75	98.77
A'–B'	98.38	98.42	98.4	98.4
B'–C'	98.78	98.74	98.73	98.75
C'–A'	98.92	98.88	98.87	98.89
A–A'	49.11	49.04	49.03	49.06
B–B'	48.86	48.88	48.87	48.87
C–C'	48.79	48.75	48.77	48.77

Table 3 Average value measured by caliper

Irregular Sample	Caliper1	Caliper2	Caliper3	Mean Caliper(mm)
A–A'	41.81	41.89	42.09	41.93
B–B'	36.07	35.97	36.14	36.06
C–C'	66.13	66.2	65.7	66.01
D–D'	44.37	44.66	44.26	44.43

Table 4 shows that the root mean square error of sample 1 is 2.5232, and the mean absolute error is 2.0356. By comparing the scanning data with the actual caliper measurement results at points A-A', B-B,' C-C,' and D-D' for sample 1 in Table 5.3, it was found that the horizontal size of the sample was more accurate, but the vertical size error was larger. The reason may be caused by the spot diameter of the infrared distance sensor (see Figure 39). As the Z coordinate increases, when the light spot shines on the object's edge, part of the light

spot passes through the object and is reflected, resulting in a measurement error at this measurement point. This results in an error in the longitudinal dimensions of the object obtained by the scanner.

Table 4 Dimension and results of sample 1

Sample 1	Mean Calliper(mm)	Scan 1 (mm)	Scan 2 (mm)	Scan 3 (mm)	$\delta1(mm)$	$\delta2(mm)$	$\delta3(mm)$	$\bar{\delta}(mm)$
A–B	79.7	79.53	79.92	79.97	0.17	−0.22	−0.27	0.22
B–C	79.16	74.45	72.65	75.33	4.71	6.51	3.83	5.016667
C–D	79.65	79.32	79.99	80.02	0.33	−0.34	−0.37	0.346667
D–A	79.24	74.52	75.63	76.06	4.72	3.61	3.18	3.836667
A'–B'	78.7	76.5	75.01	79.99	2.2	3.69	−1.29	2.393333
B'–C'	78.68	73.77	74.57	77.5	4.91	4.11	1.18	3.4
C'–D'	79.27	76.3	75.86	80.04	2.97	3.41	−0.77	2.383333
D'–A'	78.64	74.19	74.28	78.32	4.45	4.36	0.32	3.043333
A–A'	79.42	79.99	78.12	81.95	−0.57	1.3	−2.53	1.466667
B–B'	79.61	80.03	78.68	78.85	−0.42	0.93	0.76	0.703333
C–C'	79.47	80.03	79.88	78.84	−0.56	−0.41	0.63	0.533333
D–D'	79.4	79.99	79.27	81.94	−0.59	0.13	−2.54	1.086667
							RMSE	MAE
							2.52317279	2.035833

Figure 39 The light spot of the sensor captured by the camera under the dark environment

Table 5 shows that the root mean square error of sample 2 is 0.586, and the mean absolute error is 0.5391.

Table 5 Dimension and results of Sample 2

Sample 2	Mean Calliper(mm)	Scan 1 (mm)	Scan 2 (mm)	Scan 3 (mm)	$\delta1(mm)$	$\delta2(mm)$	$\delta3(mm)$	$\bar{\delta}(mm)$
A–B	75.46	76.04	75.67	74.43	−0.58	−0.21	1.03	0.606667
A–A'	50.4	50	48.39	50.23	0.4	2.01	0.17	0.86
B–B'	50.29	49.97	49.98	50.24	0.32	0.31	0.05	0.226667
C–C'	50.22	49.96	49.12	50.25	0.26	1.1	−0.03	0.463333
							RMSE	MAE
							0.586024744	0.539167

Table 6 shows that the root mean square error of sample 3 is 1.8525, and the mean absolute error is 1.6419.

Table 6 Dimension and results of Sample 3

Sample 3	Mean Calliper(mm)	Scan 1 (mm)	Scan 2 (mm)	Scan 3 (mm)	$\delta1(mm)$	$\delta2(mm)$	$\delta3(mm)$	$\bar{\delta}(mm)$
A−B	98.39	95.41	96.3	98.21	2.98	2.09	0.18	1.75
B−C	98.54	96.25	96.51	98.66	2.29	2.03	−0.12	1.48
C−A	98.77	96.62	96.94	100.05	2.15	1.83	−1.28	1.753333
A'−B'	98.4	96.6	96.13	95.14	1.8	2.27	3.26	2.443333
B'−C'	98.75	97.3	95.46	94.1	1.45	3.29	4.65	3.13
C'−A'	98.89	97.24	96.4	96.03	1.65	2.49	2.86	2.333333
A−A'	49.06	49.47	49.89	48.46	−0.41	−0.83	0.6	0.613333
B−B'	48.87	48.22	48.62	49.03	0.65	0.25	−0.16	0.353333
C−C'	48.77	49.64	49.62	49.81	−0.87	−0.85	−1.04	0.92
							RMSE	MAE
							1.85249748	1.641852

Table 7 shows that the root mean square error of the irregular sample is 2.4289, and the mean absolute error is 2.415.

Table 7 Dimension and results of irregular sample

Irregular Shape	Mean Calliper(mm)	Scan 1 (mm)	Scan 2 (mm)	Scan 3 (mm)	$\delta1(mm)$	$\delta2(mm)$	$\delta3(mm)$	$\delta(mm)$
A−A'	41.93	43.27	46.61	44.37	−1.34	−4.68	−2.44	2.82
B−B'	36.06	37.23	38.66	39.19	−1.17	−2.6	−3.13	2.3
C−C'	66.01	68.19	68.18	68	−2.18	−2.17	−1.99	2.113333
D−D'	44.43	40.83	42.52	42.66	3.6	1.91	1.77	2.426667
							RMSE	MAE
							2.428852038	2.415

The marking points only take the outline part of the irregular sample. The accuracy of contour dimensions of irregular objects is relatively high. On the contrary, as can be seen in Figure 40, a comparison between the physical image of the irregular object and the three-dimensional reconstructed model found that the details of the reconstructed model were seriously lost. The reason may be due to the insufficient accuracy of the infrared sensor itself and the too-sparse point cloud density caused by the spot size.

Figure 40 Irregular sample shape comparison

Additionally, by comparing the results of samples 1, 2, 3, and the irregular sample, it is found that the RMSE and MAE of sample 2 are smaller than samples 1, 3, and the irregular sample. The reason is that samples 1, 3, and irregular samples have sharp angular shapes, while sample 2 has a curved surface. The sharp edges of 1, 3, and the irregular sample will affect the spot reflection of the infrared sensor, thus causing measurement errors.

Table 8 shows that the combined root mean square error of samples 1,2 and 3 is 1.6539, and the mean absolute error is 1.4056. This scanning error is consistent with personal requirements for 3D scanners, such as secondary development of 3D reconstruction of small ordinary objects and digital storage of models.

Table 8 Combined results of regular sample

Regular sample	Conbined RMSE	Conbined MAE
	1.653898338	1.405617284

The cause of the 3D scanner's scanning error may also be caused by the mechanical part when it is running. During the operation of the scanner, it was discovered that the infrared sensor on the screw slide did not move entirely vertically. When lifting, the position of the sensor may change slightly due to the fit gap between the optical axis and the slider. In addition, due to defects in the manufacturing process of the trapezoidal screw, there is a slight bend in its shape, which will also cause displacement of the sensor on the slide. The above phenomenon will cause the distance error measured by the sensor to cause the error of model reconstruction directly.

V.   CONCLUSION

The root mean square error and mean absolute error of the 3D scanner built in this project for small regular and irregular objects are below 2.5232 and 2.415, respectively. The scanner built in this project is limited to small opaque objects. Based on the mechanical structure design, the maximum lifting distance of the infrared sensor is 189 mm, and the minimum measurement distance of the infrared ranging sensor is 40 mm. Therefore, the height of the scanned object cannot be higher than 189 mm, and the maximum width cannot be greater than 180 mm. In addition, the accuracy will be significantly reduced for complex sharp objects, and local details will be lost. Under these scanning limitations, it is beneficial for individuals and small institutions to use small, low-cost 3D scanners to perform three-dimensional reconstruction of regular objects for digital resource management of models.

Each electronic module of the scanner in this project is independent of each other. A production model that simultaneously builds modular electronic devices and assembles 3D scanners can be adopted in industrial mass production to make mass production more efficient. In addition, by checking the product's electronic modules, faults can be more easily found and solved by replacing the modules, simplifying the scanner's fault diagnosis process.

The scanner part is built using low-cost modular components, with a total price of 161.95 $. The bill of materials is shown in Table 9. Compared with commercial scanners on the market, it has the advantages of low cost and low installation difficulty. Its portable design in a suitcase shape provides a solution for reducing the size of industrial-grade 3D scanners.

Table 9 Bill of materials

PART NUMBER	PRICE ($)	QTY.
42BYGH48 stepper motor moter	18	2
Z- axis motor holder	8	1
Coupling	1.2	1
Lead screw	2.5	1
Support rod holder (upper end)	12	1
Support rod	2	2
Support rod holder (lower end)	12	1
Slider	12	1
Sharp infrared distance sensor (GP2Y0A41SKOF)	5.38	1
Screw nut	1	1
Lifting structure housing	15	1
Rotary table structure housing	15	1
Hinge	1.3	1
ILI8431 touch screen	10.24	1
Distance sensor housing	5	1
flange	2	1
Rotating table	5	1
Rotating motor holder	8	1
A4988 stepper motor driver	4	2
MP1584EN DC buck converter	2.2	1
SD card module	2.13	1
Arduino Mega 2560	18	1
Total costs	161.95	

This scanner still needs to be improved in some areas in the future. Regarding data transmission, an SD card is troublesome as a wired transmission method and can be enhanced to wireless transmission in the future. For example, Bluetooth transmission can be used to transfer the scanned text file directly to the user's mobile phone or computer. In addition, the infrared distance sensor can be changed to a higher-accuracy sensor to improve the scanner's accuracy. For example, using LEUZE's ODS9L2.8/L6X-1050-M12 optical triangulation distance sensor, the light spot diameter at 1050 mm is only 1.5 mm, and the measurement accuracy is 1.5% (ODS9L2.8/L6X-1050-M12 | 50147694, 2023). Therefore, this sensor's support can significantly improve the scanner's scanning accuracy. Based on the scanning speed of current scanners, single-point scanning of objects takes too long. Therefore, structured light scanning can be used instead of single-point scanning to increase the scanning speed. Combining the advantages of structured light scanners on the market, the infrared distance sensor can be replaced with a structured light projector and a camera. The camera continuously captures the structured light changes on each object's surface as it rotates on the rotating table to obtain the XYZ point cloud coordinates. The computer performs post-processing and reconstruction into a 3D model to increase scanning speed.

REFERENCE

[1]. Fontana, R., Gambino, M. C., Greco, M., Pampaloni, E., Pezzati, L., & Scopigno, R. (2003, October 13). <title>High-resolution 3D digital models of artworks</title>. SPIE Proceedings. https://doi.org/10.1117/12.501248

[2]. Javaid, M., Haleem, A., Pratap Singh, R., & Suman, R. (2021). Industrial perspectives of 3D scanning: Features, roles and it's analytical applications. Sensors International, 2, 100114. https://doi.org/10.1016/j.sintl.2021.100114

[3]. Haleem, A., Javaid, M., Singh, R. P., Rab, S., Suman, R., Kumar, L., & Khan, I. H. (2022, June). Exploring the potential of 3D scanning in Industry 4.0: An overview. International Journal of Cognitive Computing in Engineering, 3, 161–171. https://doi.org/10.1016/j.ijcce.2022.08.003

[4]. The history and introduction of CMM: the inseparable relation between CMM and GD&T. (2022, February 19). Wasy Research. https://www.wasyresearch.com/the-history-and-introduction-of-cmm-the-inseparable-relation-between-cmm-and-gd-t/

[5]. Maiman, T. H. (2018, January 23). The Laser Inventor: Memoirs of Theodore H. Maiman. Springer.

[6]. Strauss, O. (1992). Perception de l'environnement par vision en lumière structurée : segmentation des images par poursuites d'indices. http://www.theses.fr/1992MON20010

[7]. Bell, T., Li, B., & Zhang, S. (2016, February 15). Structured Light Techniques and Applications. Wiley Encyclopedia of Electrical and Electronics Engineering, 1–24. https://doi.org/10.1002/047134608x.w8298

[8]. All3DP. (2023). The Best 3D Scanners in 2023 – Buyer's Guide. All3DP Pro. https://all3dp.com/1/best-3d-scanner-diy-handheld-app-software/

[9]. ODS9L2.8/L6X-1050-M12 | 50147694. (2023). Leuze Online-Shop. https://www.leuze.com/en-us/ods9l2.8-l6x-1050-m12/50147694